Quantification of long-term and time-integrated glaciation patterns in Central Asia

Robin Blomdin*, Arjen P Stroeven, Jonathan M Harbor, Clas Hättestrand, Jakob Heyman, and Natacha Gribensk

Robin Blomdin
PhD, Geologist
Swedish Geological Survey
robin.blomdin@sgu.se

Bolin Centre for Climate Research
Department of Physical Geography
Stockholm University
robin.blomdin@natgeo.su.se

VETENSKAPSRÅDET
THE SWEDISH RESEARCH COUNCIL

Stockholm University

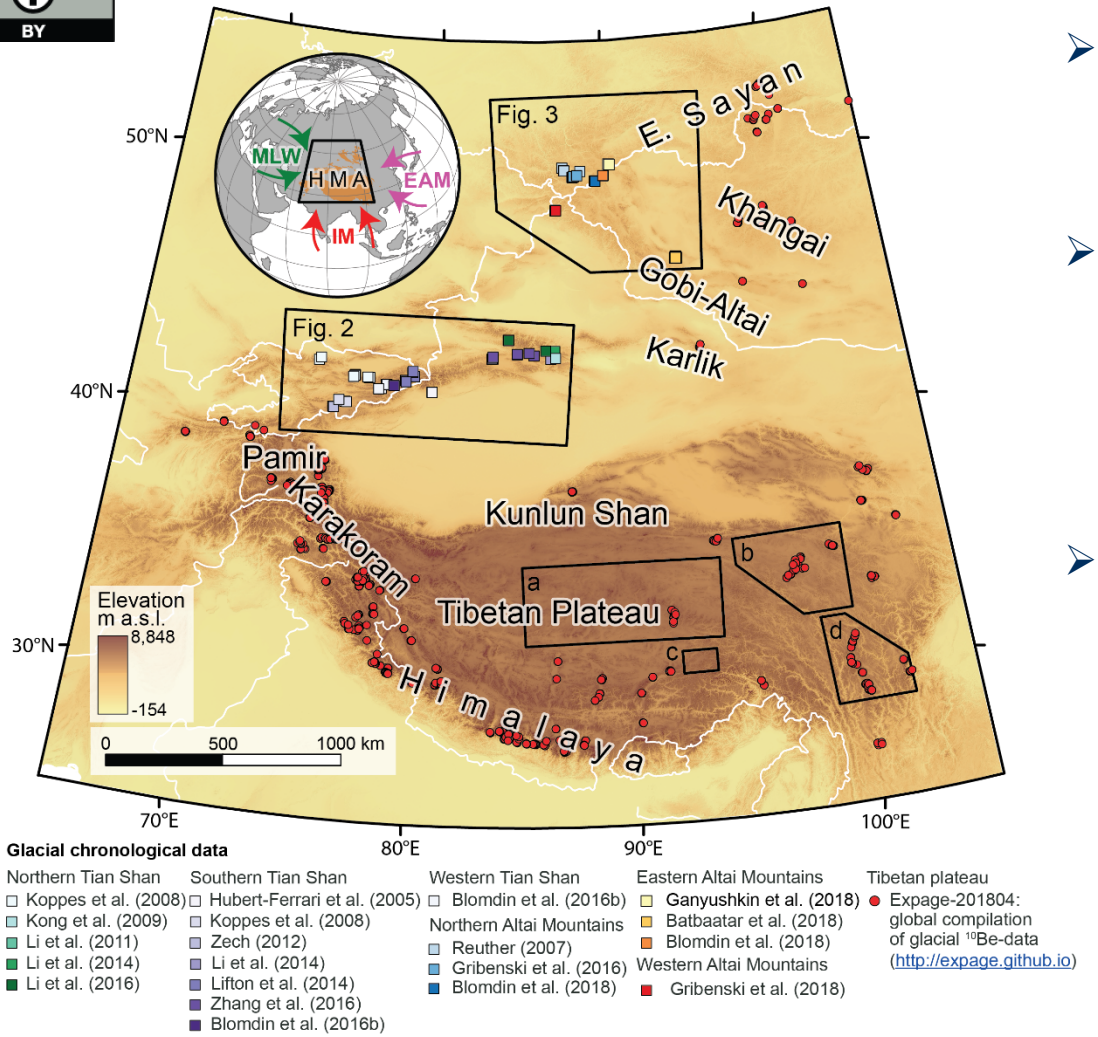

- We use a domain-wide geomorphometric analysis to investigate spatial patterns of glacial landforms.
- Our area of interest includes two large orogens in Central Asia; the Tian Shan (Fig. 2) and Altai mountains (Fig. 3), both located in the continental interior of Central Asia.
- We focus or analysis on glacial depositional landforms (e.g. marginal moraines), larger erosional landforms (e.g. glacial valleys), and available glacial chronological data, because our aim is to quantify long-term and time-integrated glaciation patterns

Fig. 1. Physiography of High-mountain Asia (HMA), the location of study areas and previously published glacial chronological data (^{10}Be surface exposure dating). Black boxes denote areas previously mapped for paleoglaciological reconstructions: **Fig. 2**) the Tian Shan (Stroeven et al., 2013), **Fig. 3**) Altai and western Sayan mountains (Blomdin et al., 2016a), a) the central Tibetan Plateau (Morén et al., 2011), b) Bayan Har Shan (Heyman et al., 2008), c) the Maidika region (Lindholm and Heyman, 2015) and d) Shaluli Shan (Fu et al., 2012). Insert map shows the location of HMA, with topography higher than 2000 m a.s.l. shaded orange and locations of major atmospheric circulation systems, SH=Siberian High-pressure system, MLW=Mid-Latitude Westerlies, IM=Indian Monsoon and EAM=East Asian Monsoon (Cheng et al., 2012).

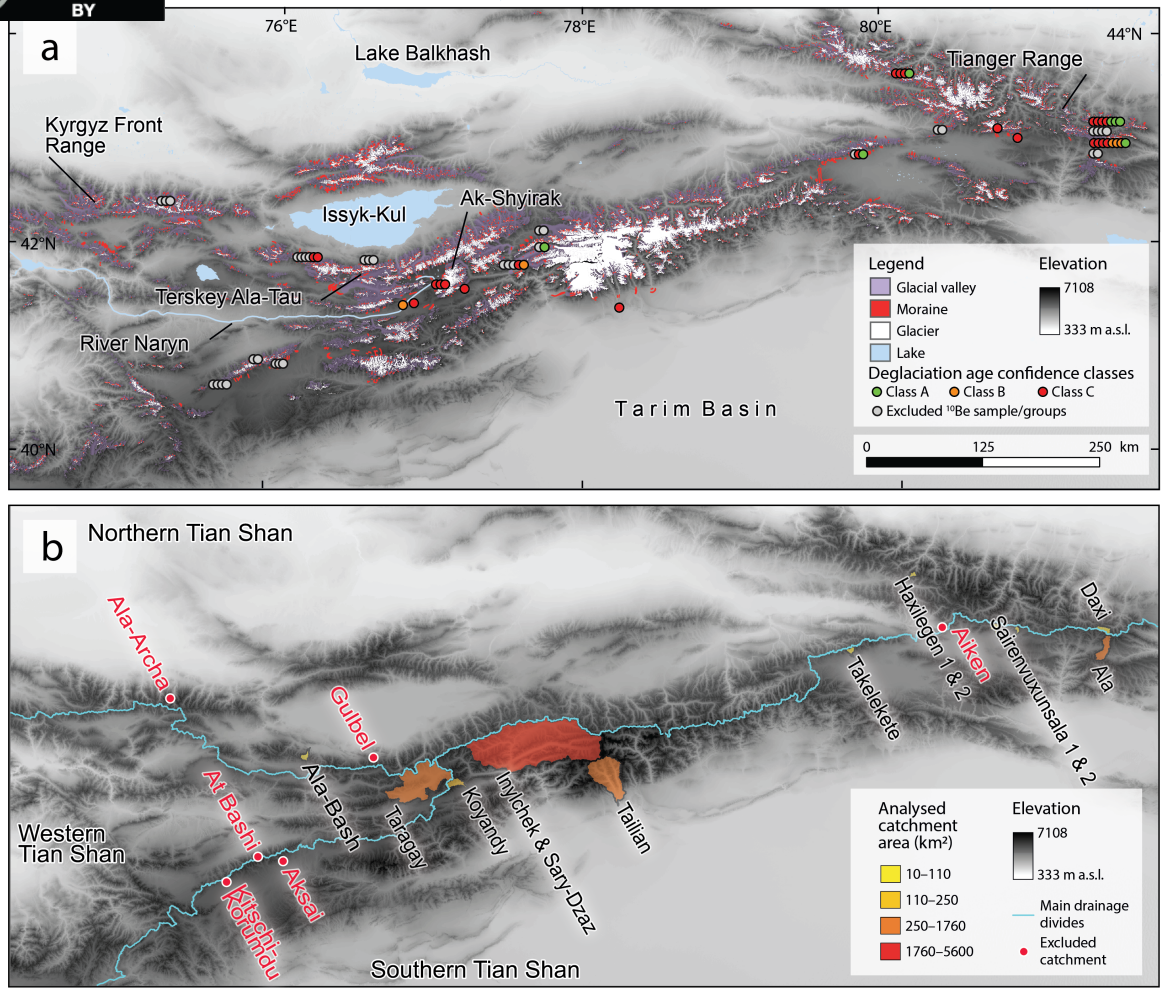

Fig. 2. a) Glacial geomorphology of the Tian Shan (Stroeven et al., 2013), the site-locations of published ^{10}Be surface exposure ages from glacial deposits and the confidence class of ^{10}Be-samples when considered as boulder groups in deriving deglaciation ages (Blomdin et al., 2018). A=good, B=moderate, and C=poor. Present-day extent of glaciers adopted from the Randolph Glacier Inventory (RGI V.6; RGI Consortium, 2017). b) Tian Shan, main drainage divides, analysed catchments (n=10) and its subdivision into three physiographic regions (northern, western, and southern).

- We focus our analysis on three different physiographic regions in the Tian Shan defined by major drainage divides,
- We also analyze formerly glaciated catchments—selected because they are intersected by cosmogenic-nuclide glacial-chronological datasets.
- We mine published datasets on the distribution of glaciers and glacial landforms, and use these datasets, together with freely available digital elevation models, to extract landform-specific hypsometric (area—elevation) distributions.

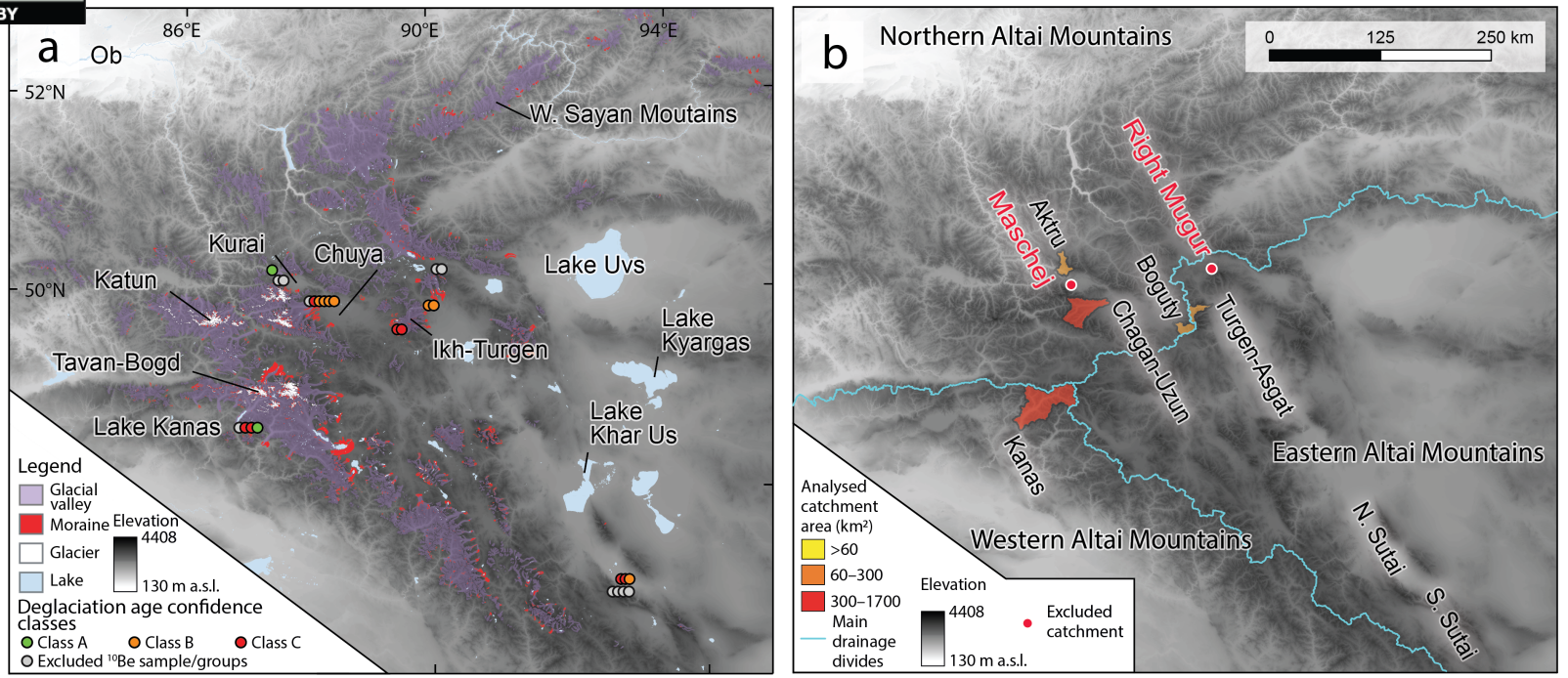

Fig. 3. a) Glacial geomorphology of the Altai Mountains (Blomdin et al., 2016a), the site-locations of published ^{10}Be surface exposure ages from glacial deposits and the confidence class of ^{10}Be-samples when considered as boulder groups in deriving deglaciation ages (Blomdin et al., 2018). A=good, B=moderate, and C=poor. Present-day extent of glaciers adopted from the Randolph Glacier Inventory (RGI V.6; RGI Consortium, 2017). b) Altai Mountains, main drainage divides, analysed catchments (n=7) and its subdivision into three physiographic regions (northern, eastern, and western).

- We also include in our analysis, three different physiographic regions in the Altai Mountains defined by major drainage divides,
- We also analyze formerly glaciated catchments—selected because they are intersected by cosmogenic-nuclide glacial-chronological datasets.
- We mine published datasets on the distribution of glaciers and glacial landforms, and use these datasets, together with freely available digital elevation models, to extract landform-specific hypsometric (area—elevation) distributions.

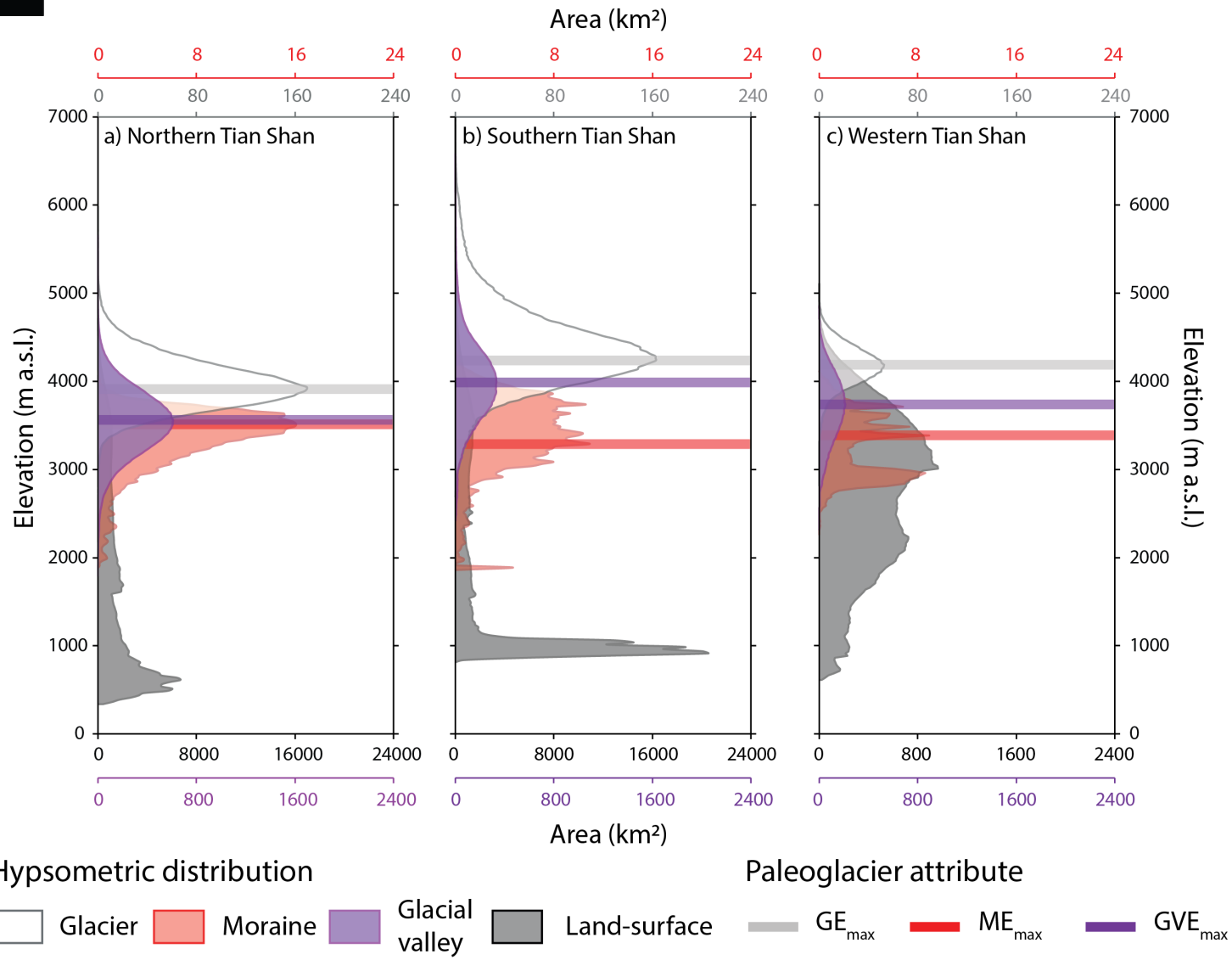

Fig. 4. Hypsometric distributions of glaciers, moraines, glacial valleys, and total land-surface, and inferred (paleo)glacier attributes, for a) northern, b) southern, and c) western Tian Shan. GE_{max} = Glacier Elevation Maximum, ME_{max} = Moraine Elevation Maximum, GVE_{max} = Glacial Valley Elevation Maximum.

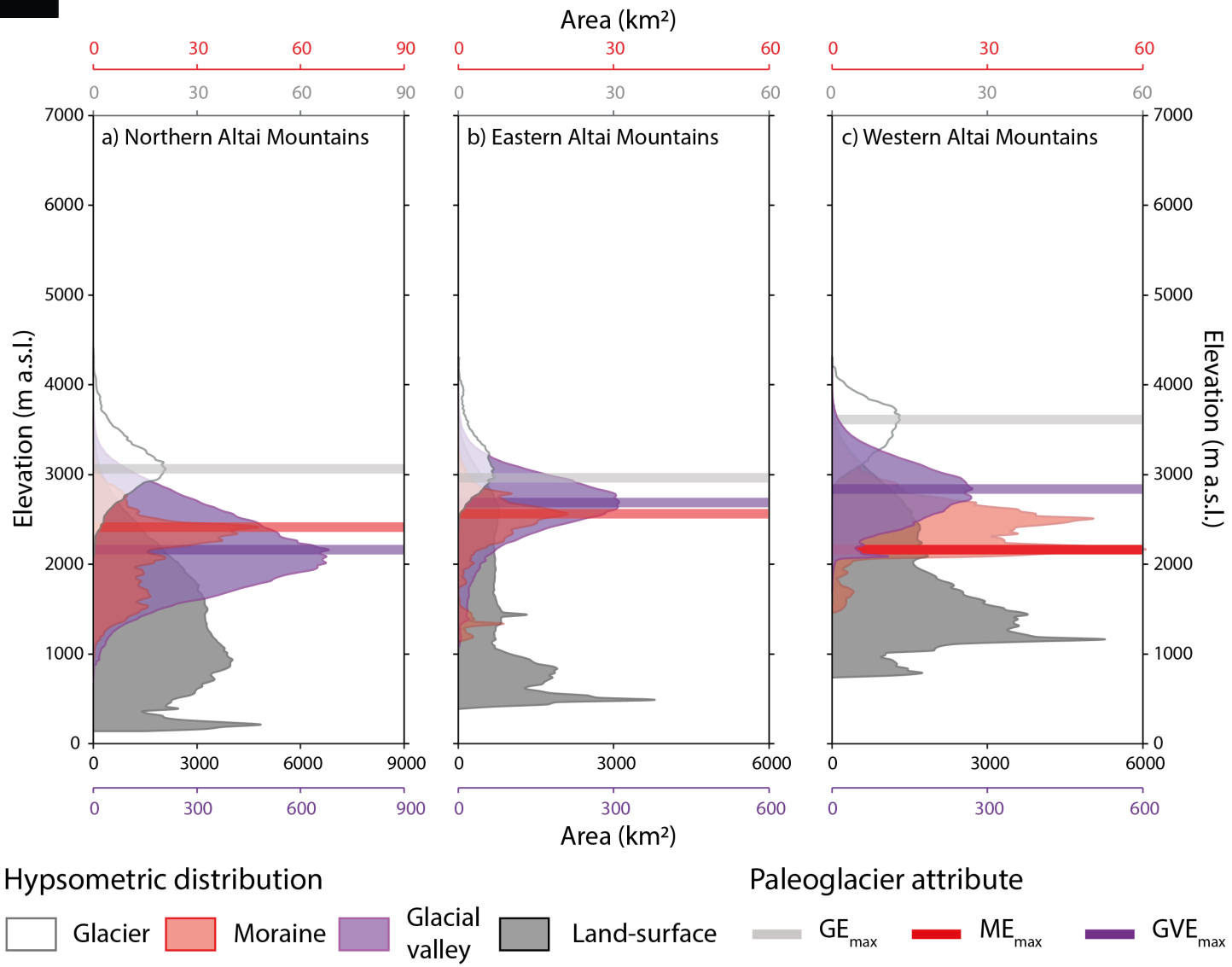

Fig. 7. Hypsometric distributions of glaciers, moraines, glacial valleys, and total land-surface, and inferred (paleo)glacier attributes, for a) northern, b) eastern, and c) western Altai Mountains. GE_{max} = Glacier Elevation Maximum, ME_{max} = Moraine Elevation Maximum, GVE_{max} = Glacial Valley Elevation Maximum.

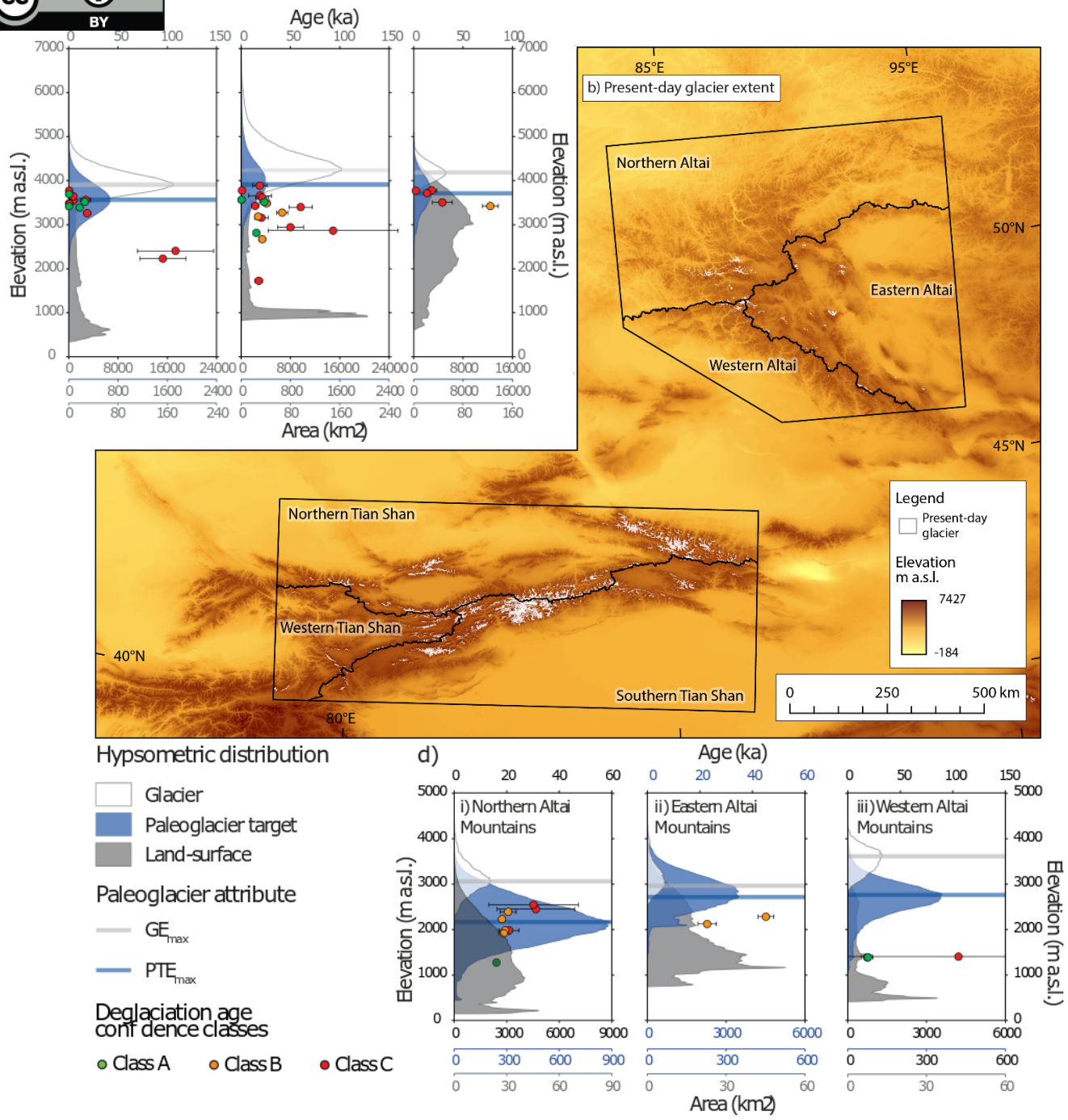

- Hypsometric peaks for modern glaciers (i.e. median glacier elevations) show pronounced spatial gradients; increasing elevations from the northern to the southern Tian Shan, and increasing median elevations from the northern to both the southeastern and southwestern Altai Mountains.

Stockholm University

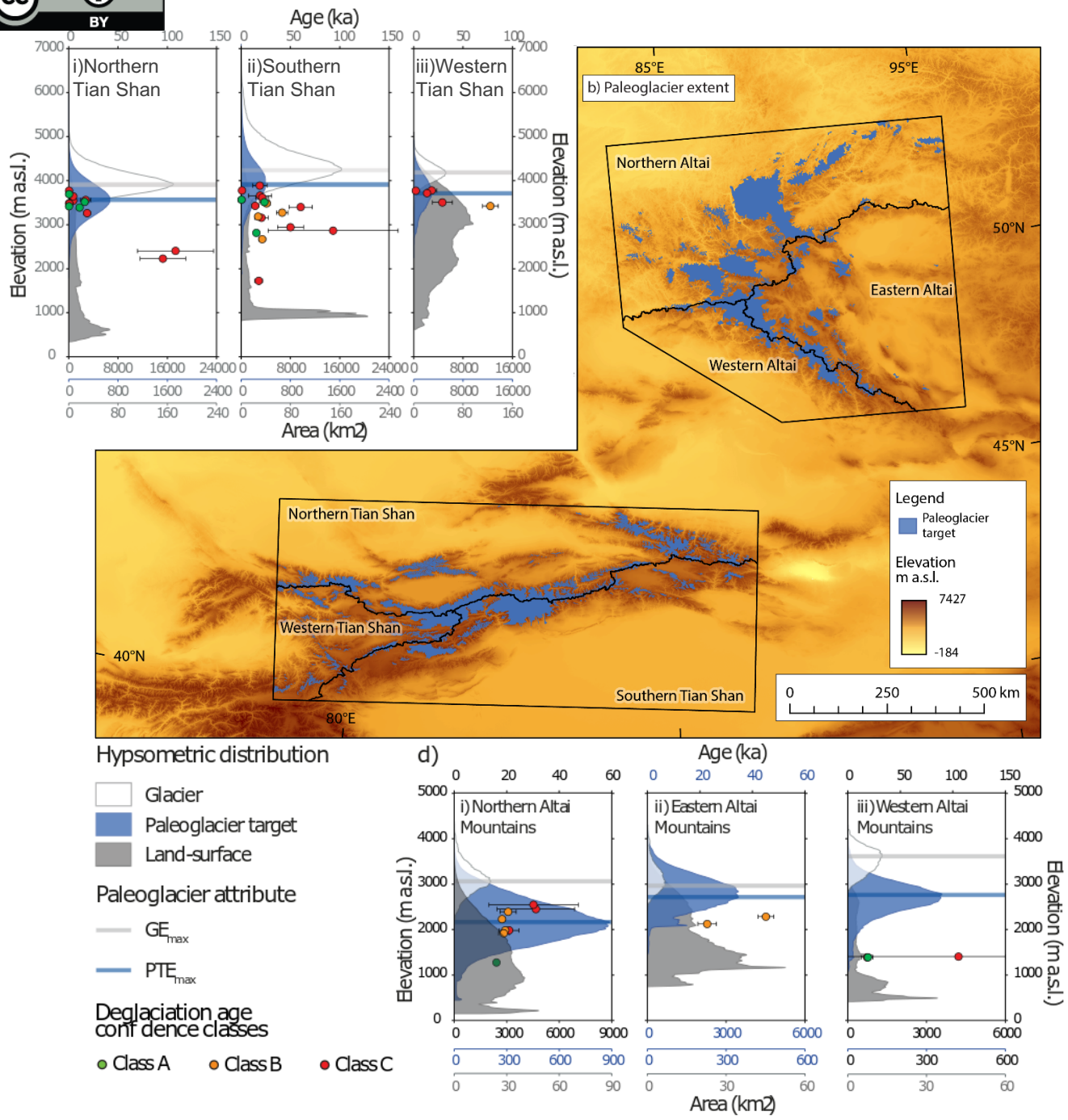

- A similar pattern can be observed in the paleorecord; reconstructed long-term and time-integrated glaciation patterns, also show pronounced spatial gradients, equivalent to modern median glacier elevation patterns.

Stockholm University

Long-term, time-integrated spatial patterns of paleoglaciation

- Clear modern-day ELA gradient from the southern/eastern cold/dry regions to the northern cold/wet regions
  - This is interpreted to reflect topographic barrier effects and decreasing modern precipitation rates (i.e. increasing continentality), as a result of a weakening of the Mid-latitude Westerlies, across the main axes of the two mountain systems.
- Similar gradients observed for the reconstructed paleoglacier targets. Similar long-term precipitation gradients as today?
  - This observation indicates that during former periods of glaciation, maximum paleoglacier extents—reconstructed by delineating the extent of glacial depositional and erosional landforms (formed over one-to-several glacial cycles, over >100 thousand years)—were correspondingly controlled by a westerly-sourced moisture supply, and was thus affected by precipitation patterns similar to those of today.

References

Arendt, A. et al. (2015). Randolph Glacier Inventory – A Dataset of Global Glacier Outlines: Version 5.0 - GLIMS Technical Report.

Blomdin, R. et al. (2016a). Glacial geomorphology of the Altai and Western Sayan Mountains, Central Asia. J. Maps 12, 123–136.

Blomdin, R. et al. (2016b). Evaluating the timing of former glacier expansions in the Tian Shan: a key step towards robust spatial correlations. Quat. Sci. Rev. 153, 78–96.

Blomdin, R. et al. (2018). Timing and dynamics of glaciation in the Ikh Turgen Mountains, Altai region, High Asia. Quat. Geochr. 47, 54-71.

Blomdin, R. et al. (in prep.). Topographic and climatic controls on glaciation across Central Asia.

Gribenski, N. et al. (2016). Complex patterns of glacier advances during the Lateglacial in the Chagan-Uzun Valley, Russian Altai. Quat. Sci. Rev. 149, 288–305.

Gribenski, N. et al. (2018). Re-evaluation of MIS 3 glaciation using cosmogenic radionuclide and single grain luminescence ages, Kanas Valley, Chinese Altai. Journal of Quaternary Science 33, 55-67.

Heyman, J. et al. (2011). Too young or too old: Evaluating cosmogenic exposure dating based on an analysis of compiled boulder exposure ages. Earth Planet. Sci. Lett. 302, 71–80.

Hijmans, R.J. et al. (2005). Very high resolution interpolated climate surfaces for global land areas. Int. J. Climatol. 25, 1965–1978.

Hubert-Ferrari, A. et al. (2005). Irregular earthquake cycle along the southern Tianshan front Aksu area, China. J. Geophys. Res. B Solid Earth 110, 1–18.

Kong, P. et al. (2009). Late Quaternary glaciation of the Tianshan, Central Asia, using cosmogenic ^{10}Be surface exposure dating. Quat. Res. 72, 229–233.

Koppes, M. et al. (2008). Late Quaternary glaciation in the Kyrgyz Tien Shan. Quat. Sci. Rev. 27, 846–866.

Laskar, J. et al. (2004). A long-term numerical solution for the insolation quantities of the Earth. Astron. Astrophys. 428, 261–285.

Li, Y.K. et al. (2016). Cosmogenic ^{10}Be constraints on Little Ice Age glacial advances in the eastern Tian Shan, China. Quat. Sci. Rev. 138, 105–118. doi:10.1016/j.quascirev.2016.02.023

Li, Y.K. et al. (2014). Timing and extent of Quaternary glaciations in the Tianger Range, eastern Tian Shan, China, investigated using ^{10}Be surface exposure dating. Quat. Sci. Rev. 98, 7–23. doi:10.1016/j.quascirev.2014.05.009

Li, Y.K. et al. (2011). Cosmogenic nuclide constraints on glacial chronology in the source area of the Urumqi River, Tian Shan, China. J. Quat. Sci. 26, 297–304.

Lifton, N. et al. (2014). Constraints on the late Quaternary glacial history of the Inylchek and Sary-Dzaz valleys from in situ cosmogenic ^{10}Be and ^{26}Al, eastern Kyrgyz Tian Shan. Quat. Sci. Rev. 101, 77–90.

Nuimura, T. et al. (2015). The GAMDAM Glacier Inventory : a quality controlled inventory of Asian glaciers. Cryosph. 9, 849–864.

Reuther, A. (2007). Surface exposure dating of glacial deposits from the last glacial cycle – evidence from the eastern Alps, the Bavarian Forest, the southern Carpathians and the Altai Mountains.

Stroeven, A.P. et al. (2013). Glacial geomorphology of the Tian Shan. J. Maps 9, 505–512.

Thompson, L.G. et al. (1997). Tropical climate instability: The last glacial cycle from a Qinghai-Tibetan ice core. Science 276, 1821–1825.

Wünnemann, B. et al. (2007). Responses of Chinese desert lakes to climate instability during the past 45,000 years. Dev. Quat. Sci. 9, 11–24.

Zech, R., 2012. A late Pleistocene glacial chronology from the Kitschi-Kurumdu Valley, Tien Shan (Kyrgyzstan), based on ^{10}Be surface exposure dating. Quat. Res. 77, 281–288.

Zhang, M. et al. (2016). Late Quaternary glacial history of the Nalati Range, central Tian Shan, China, investigated using 10Be surface exposure dating. J. Quat. Sci. 31, 659–670.